sustainability

MDPI

Article

Efficient Degradation of Rhodamine B Dye through Hand Warmer Heterogeneous Activation of Persulfate

Tiantian Ye [1], Lihong Liu [1], Yilin Wang [1], Jianqiang Zhang [1,*], Zhenxing Wang [1,*], Cong Li [1] and Haoyu Luo [2]

[1] South China Institute of Environmental Sciences, Ministry of Ecology and Environment, Guangzhou 510655, China
[2] Guangdong Industrial Contaminated Site Remediation Technology and Equipment Engineering Research Center, School of Environmental Science and Engineering, Guangdong University of Technology, Guangzhou 510006, China
* Correspondence: zhangjianqiang@scies.org (J.Z.); wangzhenxing@scies.org (Z.W.)

Abstract: In this study, an innovative method for RhB (Rhodamine B) degradation in a persulfate (PS) and hand warmer heterogeneous activation system was investigated. The hand warmer showed better catalytic performance and excellent reusability in terms of PS activation. The reaction rate constants of RhB removal in the hand warmer/PS process (0.354 min^{-1}) were much faster than those in other PS- and Fe-related processes (0.010–0.233 min^{-1}) at pH 7. The iron in the hand warmer is the main active ingredient to catalyze PS, and activated carbon, salt, and H^+/OH^- accelerate the activated reaction due to the formation of micro-batteries in the solution. Moreover, the catalyst of the hand warmer showed excellent stability and reusability with a low level of iron leaching. This new, effective, inexpensive, repeatable, and environmentally friendly catalyst combined with PS has promising prospects for the removal of dyes from industrial wastewater.

Keywords: heterogeneous activation; persulfate; hand warmer

Citation: Ye, T.; Liu, L.; Wang, Y.; Zhang, J.; Wang, Z.; Li, C.; Luo, H. Efficient Degradation of Rhodamine B Dye through Hand Warmer Heterogeneous Activation of Persulfate. *Sustainability* **2023**, *15*, 13034. https://doi.org/10.3390/su151713034

Academic Editor: Domenico Licursi

Received: 24 July 2023
Revised: 19 August 2023
Accepted: 25 August 2023
Published: 29 August 2023

1. Introduction

As one of the promising, efficient, practically feasible, and environmentally friendly methods for in situ oxidation of organic contaminants, advanced oxidation processes (AOPs) have drawn increasing attention recently [1,2]. Due to their long half-life, high solubility, and high redox potential (2.5–3.1 V), sulfate radical-induced AOPs are regarded as an emerging and alternative technology [3–5]. Persulfate (PS) is commonly used as the source of sulfate radical ($SO_4^{\bullet-}$) and presents low oxidative potential for the degradation of organic compounds by itself. However, PS can be activated by UV irradiation, heating, transition metals, ultrasound, activated carbon, and so on, and then generate $SO_4^{\bullet-}$ to trigger the advanced oxidation processes [6,7].

Transition metals are usually used in the AOPs among the various activation approaches due to their convenience and efficiency. As one of the common transition metals, iron (Fe) is the most studied and reported as the activator for PS because of its effectiveness, non-toxicity, and environmental friendliness [8–10]. Previously, most studies were focused on homogenous processes (ferrous ion Fe^{2+}, soluble) for PS activation. Ji et al. found that the degradation of ciprofloxacin in groundwater through the Fe^{2+}-activated PS process was more efficient than sulfamethoxazole at near-neutral pH (pH 6.0) [11]. Although PS/Fe^{2+} typically performs well at a low pH, its treatment efficiency dramatically drops with an increase in pH [12]. To address this pH issue, zero-valent iron (Fe^0, heterogeneous process) has been reported to substitute PS/Fe^{2+} (homogenous process). For instance, Deng et al. evaluated Fe^0 as an alternative iron source to activate PS and found that the Fe^0/PS system was effective for acetaminophen degradation in a broader pH range from 3 to 8.5 [13]. Indeed, Fe^0/PS has a wider working pH range when compared to the PS/Fe^{2+} process. Unfortunately, insoluble ferric products are formed in the Fe^0/PS process, which

blocks the cycling of Fe(III)/Fe(II) and incurs additional operation costs for the removal of iron sludge.

To minimize these disadvantages in the Fe^0/PS process, more effective heterogeneous activators like Fe-containing zeolites, clays, or ferrites for PS have been explored [14–16]. Zhang et al. prepared copper-ferrite-decorated multi-walled carbon nanotube magnetic nanoparticles as catalysts for the degradation of diethyl phthalate and showed high catalytic activity, stability, and reusability in target compound removal [14]. The use of novel heterogeneous catalysts is an emerging and promising alternative with the advantages of a wider working pH range and reusability of iron reagents.

The hand warmer is a commodity that includes heat materials in a non-woven fabric bag and can expel cold, retain warmth, and promote the microcirculation of the body to relieve pain and detumescence [17,18]. The heating material is the main exothermic fraction of the hand warmer and is made up of iron powder, vermiculite, activated carbon, and salt. Generally, the mass percentage composition of the commercial hand warmer is 70~85% for iron powder, 10~20% for vermiculite, 1~10% for activated carbon, and a small amount of NaCl. The hand warmer is self-heated through an iron oxidation reaction, based on the corrosion of iron in moist air. The oxidation rate of iron under natural conditions is slow. To accelerate the corrosion of iron, iron powder instead of a chunk of iron is used because the large surface area of the fine powder greatly speeds up the oxidation reaction. Additionally, the activated carbon helps to bring oxygen and water to the iron particles through adsorption. Therefore, the activated carbon and salt, together with the iron and water, form batteries to promote the reaction in ambient conditions.

Iron powder, vermiculite, and activated carbon are also commonly used in environmental practices. As mentioned, iron is an efficient activator of PS oxidation for organic contaminants. Furthermore, activated carbon can also catalyze PS oxidation. Yang et al. found that PS can interact with activated carbon surface and then produce $SO_4^{\bullet-}$ or $HO^{\bullet}$ to oxidize Azo dye in water [19]. Consequently, the heating material within the hand warmer offers an interesting alternative for activating PS. However, there are few reports concerning the application of the heating material within the hand warmer in the degradation of organic contaminants by PS.

Above all, the heating materials within the hand warmer are expected to be efficient in the catalytic activation of PS. The objectives of the present study are as follows: (1) to investigate the ability of the hand warmer to activate PS for the degradation of Rhodamine B (RhB), (2) to characterize the mechanisms of PS catalyzed by the hand warmer, (3) to identify the dominant active species in the PS/hand warmer system, (4) to explore the reusability of the hand warmer. In this study, the unused hand warmer and used hand warmer are called hand warmer and oxidized hand warmer, respectively, because the process of using the hand warmer is essentially an oxidation process.

2. Materials and Methods

2.1. Chemicals

The Rhodamine B (RhB, $C_{28}H_{31}ClN_2O_3$, 479.02 g/mol) and potassium persulfate ($K_2S_2O_8$, 270.32 g/mol) were provided by Sinopharm Chemical Reagent Co., Ltd. (Shanghai, China). The hand warmer used as the catalytic agent was purchased from Alibaba (Shanghai, China). The spin-trapping agent, 5,5-dimethyl-pyrroline-N-oxide (DMPO), was obtained from Aladdin, China. All the other reagents used in this study such as tert-butylalcohol (TBA) and ethanol (EtOH) were obtained from Guangzhou chemical reagent factory, China. All chemicals were of analytical grade or higher and used as received without further purification. The water used in all experiments was purified using a Milli-Q system.

2.2. Characterization of Hand Warmer

X-ray powder diffraction (XRD) measurement was carried out on an X-ray diffractometer (XRD, Brucker D8, Karlsruhe, Germany) with Cu-Kα radiation (40 kV, 40 mA) over

the 2θ range from 5° to 90° at a speed of 5°/min. The structure of the hand warmer was investigated with a scanning electron microscope (SEM, FEI Inspect F50, Thermo Fisher, Waltham, MA, USA), and the elemental composition was determined through energy-dispersive spectrometry (EDS) using an energy-dispersive X-ray spectrometer (FEIQ45, Brucker, Germany) attached to the SEM instrument. The surface chemical states of the elements were investigated through X-ray photoelectron spectroscopy (XPS) (Escalab 250xi, Thermo Fisher, Waltham, MA, USA) using an Al K Alpha X-ray source with 200 W power, and the spectra were collected with a fixed retarding ratio mode at a band-pass energy of about 30 eV. Fourier transform infrared (FTIR) spectroscopy (iS5, Thermo Nicolet, Madison, WI, USA) was used to detect the chemical groups on the surface of the catalysts.

2.3. Experimental Procedure and Analyses

Unless otherwise specified, the degradation of RhB was carried out in a 250 mL beaker at room temperature (25.0 ± 0.2 °C) and pH (pH = 4.5 ± 0.2) with an initial RhB concentration of 100 mg/L. In each experiment, 100 mL RhB solution was placed in a beaker, followed by adding a specified amount of PS and catalyst. Then, the suspension was stirred at a constant speed. At defined time intervals, 1 mL of the reaction solution was withdrawn and filtered for analysis of RhB using a UV–Vis spectrometer (DR5000, Hach, Loveland, CO, USA) at the maximum wavelength of 554 nm.

To evaluate the reusability of the catalytic agent, the used catalysts were collected, washed, dried, and reused for the next reaction under the same experimental conditions. The reusability test was initiated immediately by adding 0.02 g recycled catalyst, 100 mL 100 mg/L RhB (pH = 4.5 ± 0.2), and 3 mM PS. The amount of leached iron in the suspension was determined through Inductively Coupled Plasma-Atomic Emission Spectrometry (ICP-OES 700, Agilent Technologies, Palo Alto, CA, USA). The total organic carbon (TOC) remaining in the solution was measured using a Jena multi N/C 3100 TOC analyzer. Two sets of quenching experiments were conducted to determine the radical species in the catalytic system using TBA and EtOH as the radical scavengers. In addition, the free radicals were trapped with 5,5-dimethyl-1-pyrroline N-oxide (DMPO) and detected using an electron paramagnetic resonance (EPR) spectrometer (A300 EMXplus-10/12, Brucker, Karlsruhe, Germany). The settings for the EPR spectrometer were center field at 3510 G, sweep width at 100 G, modulation amplitude at 1 G, and conversion time at 20 ms.

3. Results and Discussions

3.1. Characterization of Hand Warmer

Figure 1 presents SEM and corresponding EDS images of the hand warmer. As can be seen from Figure 1a, the raw material of the hand warmer possessed a bulk-like microscopic morphology and a relatively coarse surface, mainly consisting of Fe, C, O, and Si. Figure 1b shows the SEM-EDS images of the hand warmer oxidized in ambient conditions, which also presented an irregular bulk-like shape and had a smaller size when compared to the raw material. Furthermore, the hand warmer contained more oxygen when oxidized in ambient conditions according to the EDS analysis. The XRD patterns of the hand warmer are shown in Figure 2. The peaks at values of about 44.673°, 65.021°, and 82.333° correspond to the diffraction of the (110), (200), and (211) crystal planes of iron in the raw material of the hand warmer, respectively (Figure 2a). When the hand warmer was oxidized in ambient conditions, the characteristic diffraction peaks of iron disappeared and other clear peaks associated with impurities like carbon were observed in the XRD pattern (Figure 2b).

The XPS spectrum of the hand warmer (Figure 3a) indicates the existence of Fe, O, C, Cl, Si, and so on, which is in accord with the results of EDS. To reveal the iron species, the Fe 2p regions (Figure 3b,d) were analyzed. For the hand warmer (Figure 3b), the Fe 2p spectra curve fitting shows that Fe^{3+} species are present on the surface. The binding energy value of 724.8 eV for the Fe^{3+} $2p_{1/2}$ peak agrees with the previous reports [20,21]. After being exposed to air, the surface of the material is oxidized, and large numbers of ferric compounds are formed. Besides the Fe^{3+} $2p_{3/2}$ peak and Fe^{3+} $2p_{1/2}$ peak at 711.1

and 724.8 eV, the Fe 2p spectra of the oxidized hand warmer show the satellite Fe^{3+} peak at 718.9 eV and 733.4 eV [20,21]. C1s spectra were also obtained to exhibit the details of functional groups as shown in Figure 3c,e, and the binding energy values 288.8 eV, 286.7 eV, 285.6 eV, and 284.7 eV, correspond to COOH, C=O, C-O, and C-C (-CH, CH_2, CH_3) groups, respectively [22,23]. The results of XPS suggested that there was no Fe^0 on the surface of the hand warmer since the Fe^0 was easily oxidized and multitudinous carbon groups such as COOH, C-O, and C-C (-CH, CH_2, CH_3) have been verified to exist on the surface of materials.

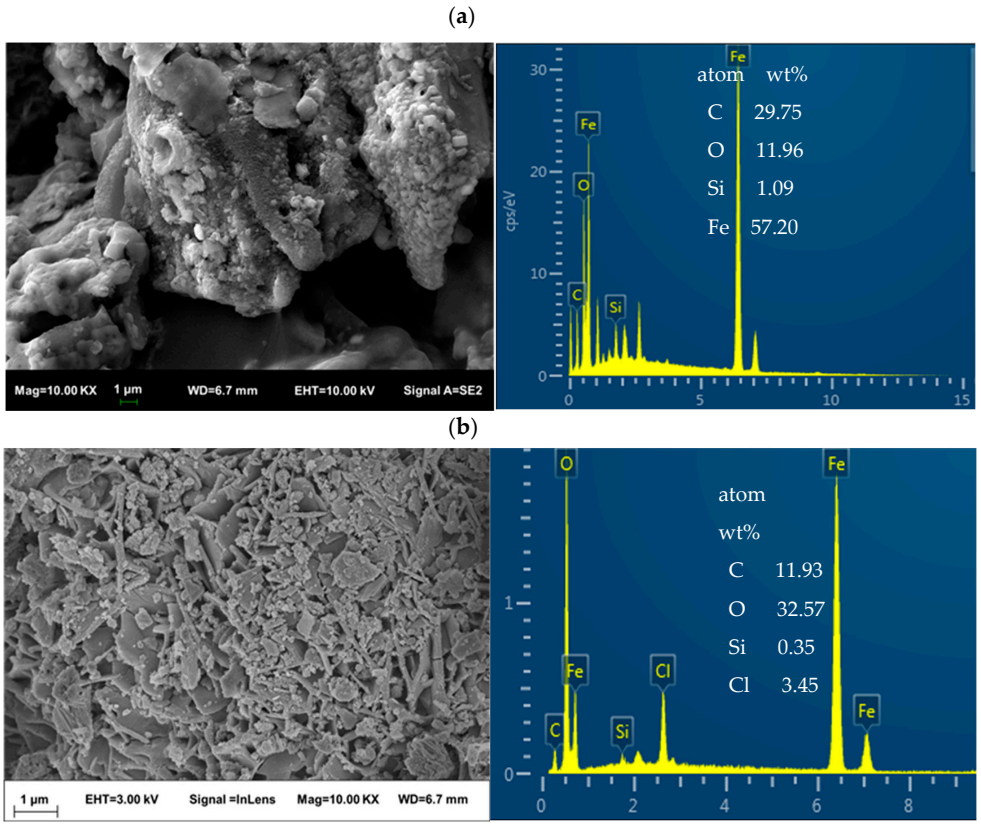

Figure 1. SEM and corresponding EDS images of (**a**) the hand warmer and (**b**) oxidized hand warmer in ambient conditions.

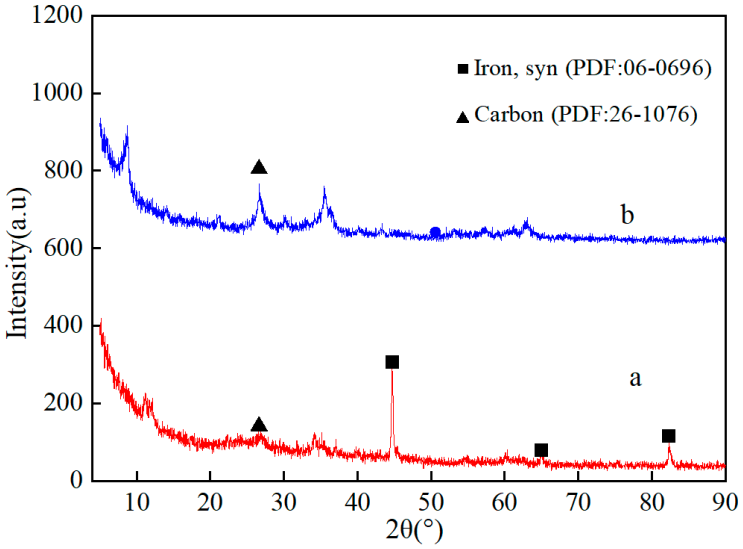

Figure 2. The XRD pattern of (**a**) the hand warmer and (**b**) oxidized hand warmer.

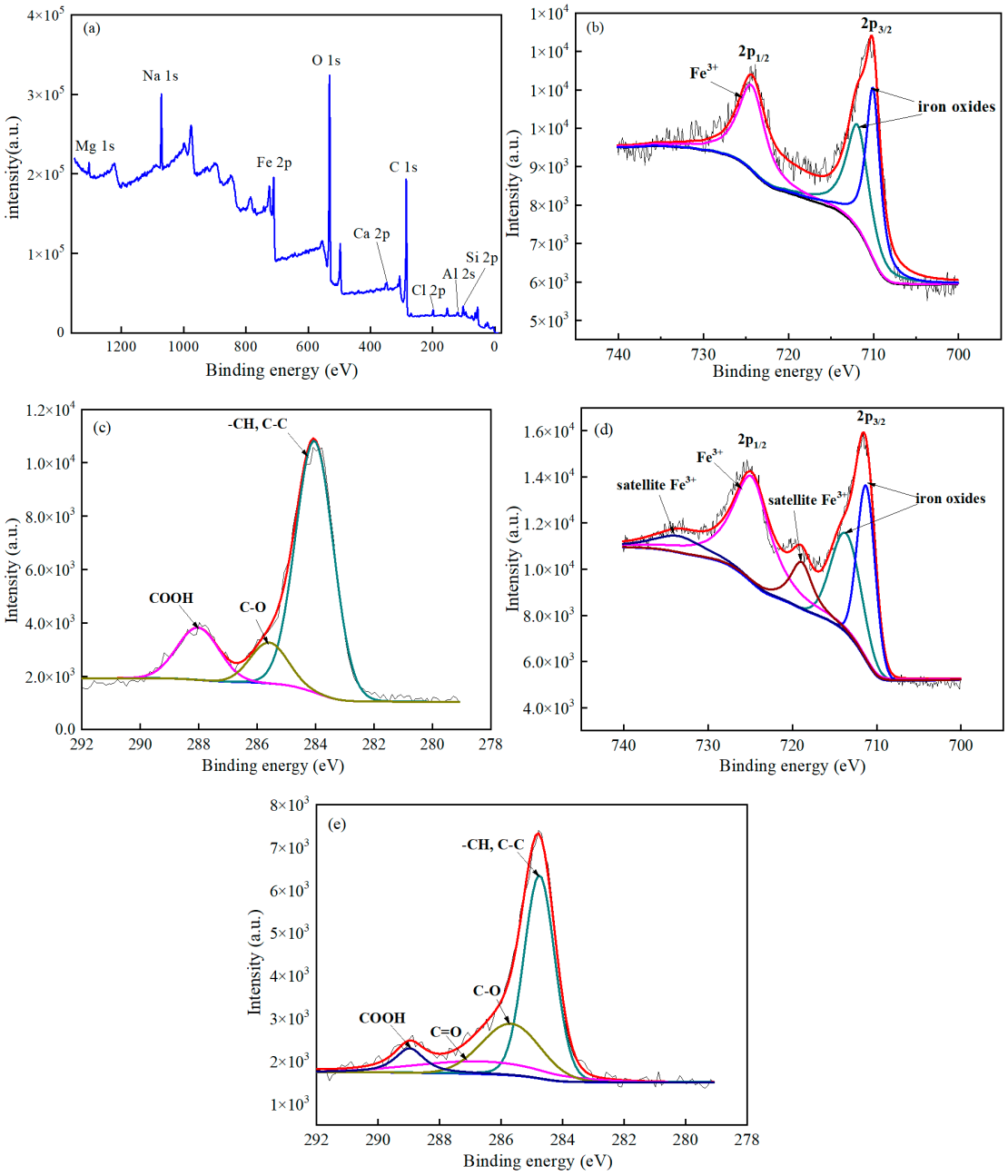

Figure 3. XPS profiles of the surface of the hand warmer and oxidized hand warmer. (**a**) Full-range XPS spectra of hand warmer, (**b**) Fe 2p spectra of hand warmer, (**c**) C1s spectra of hand warmer, (**d**) Fe 2p spectra of oxidized hand warmer, (**e**) C1s spectra of oxidized hand warmer.

As shown in Figure 4, the FTIR spectra for the hand warmer and oxidized hand warmer were recorded in the range of 400–4000 cm^{-1}. In the spectra of the hand warmer, there is an obvious absorption peak at 1003.5 cm^{-1} corresponding to the C-O group [24,25]. After oxidization, the intensity of the C-O group for the hand warmer was significantly enhanced. In addition, the adsorption broadband at 3000~3500 cm^{-1} appears, which represents the OH group [26]. The increase in the C-O group and OH group could further verify that the hand warmer was oxidized. It is noted that the spectra of the oxidized hand warmer at 400–700 cm^{-1} show two absorption bands. The first band (v_1) is around 400 cm^{-1} and the second (v_2) is around 600 cm^{-1} [27]. According to the geometrical configuration of the oxygen nearest neighbors, the v_1 band is attributed to the stretching vibration of octahedral complexes and the v_2 band to that of tetrahedral complexes [26]. Further, the

v_1 band is due to the vibrations of Si-O-Si or O-Si-O bending, and the v_2 band is due to the Fe-O complex present at tetrahedral sites [27–30]. In the spectra of the oxidized hand warmer, the absorption band at 561.8 cm^{-1} corresponds to the Fe-O group and the band at 422.77 cm^{-1} to the Si-O-Si or O-Si-O bending in vermiculite [30]. Nevertheless, there is no obvious absorption peak around 600 cm^{-1} for the hand warmer, while the absorption band at 429.56 cm^{-1} remains, corresponding to the Si-O-Si or O-Si-O group.

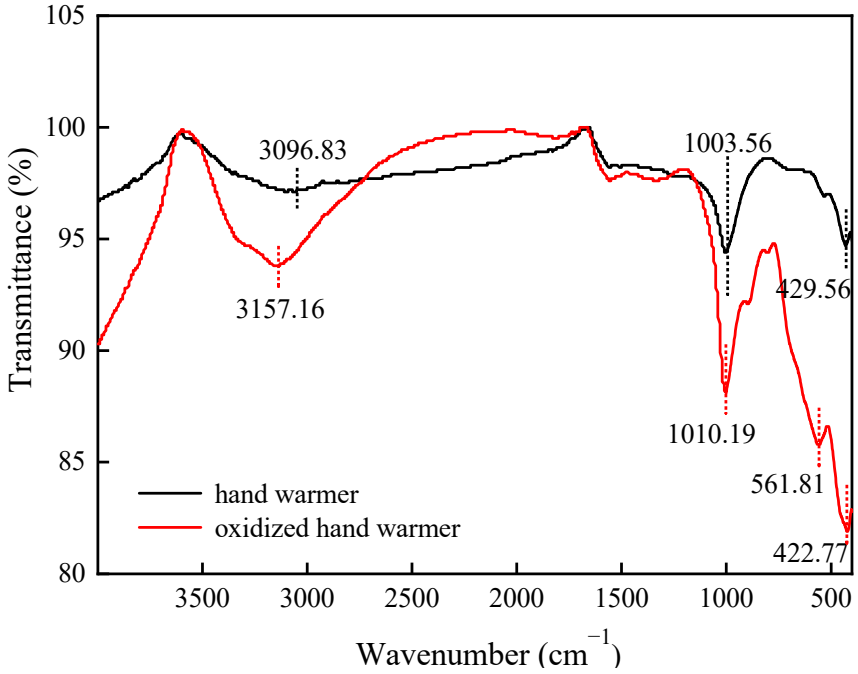

Figure 4. FTIR spectra of hand warmer and oxidized hand warmer.

3.2. Catalytic Activity of Hand Warmer

The catalytic activity of the hand warmer was investigated by performing the degradation experiments of RhB, which were carried out to compare the decolorization efficiencies of various processes at room temperature (T = 25.0 ± 0.2 °C) and pH (pH = 4.5 ± 0.2) with an initial RhB concentration of 100 mg/L. The kinetics of RhB degradation in different systems are presented in Figure 5. Except for the PS/dark and PS/hand warmer/dark systems, which were in unlit ambient conditions, the experiments were conducted under indoor light. As shown in Figure 5, RhB was hardly affected by the adsorption of the hand warmer, and the removal of RhB was only 6.8%. The addition of PS could induce slight degradation (25.7% in 30 min) of RhB in the absence of a catalyst, which verified that PS itself presented a low oxidative potential for the degradation of RhB, while the combination of PS and the hand warmer could greatly enhance the degradation efficiency of RhB to more than 99% within 30 min, due to some active species being produced in this system. Moreover, the degradation of RhB by the PS/hand warmer could be well simulated by a pseudo-first-order rate within the first 7 min (Figure S1). The apparent rate constant for the process of hand warmer/PS is 36.97 × 10^{-2} min^{-1}. Similarly, the degradation of RhB was only 24.6% in the PS/oxidized hand warmer system. These results reflect that after being oxidized, the hand warmer was inactivated and could not initiate PS to produce more active species because the Fe^0 disappeared and the Fe-O group emerged during oxidation according to the XRD, XPS, and FTIR analysis. Considering that the RhB molecule can absorb visible light to produce the excited state of the dye, irradiation by visible light may enhance the degradation of RhB. Control experiments of PS/dark and PS/hand warmer/dark systems were also employed. Little variation in RhB decolorization was observed in the absence of visible light irradiation within 30 min, illustrating that the irradiation by the indoor visible light had no significant effect on RhB degradation.

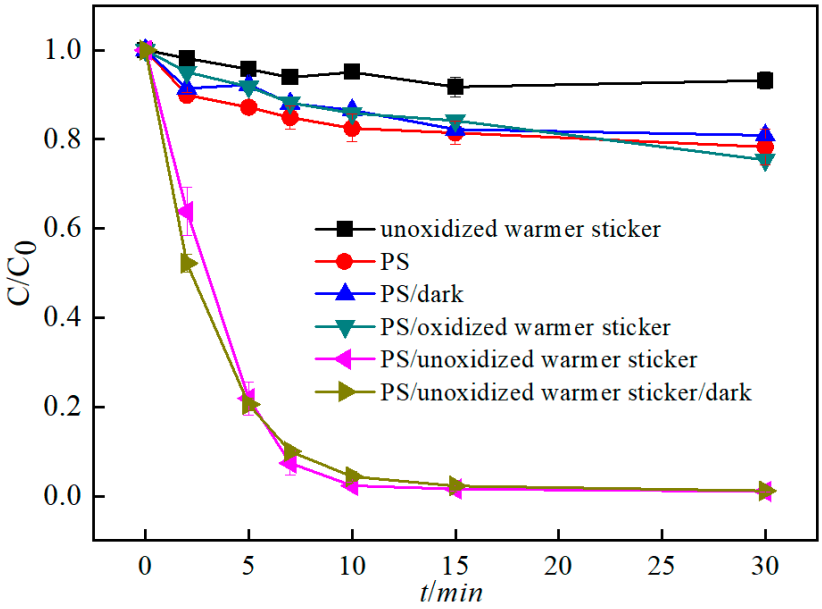

Figure 5. Decolorization of RhB under different reaction systems (hand warmer, PS, PS/dark, PS/oxidized hand warmer, PS/hand warmer, PS/hand warmer/dark).

Given that there are certain differences in the component contents of various substances (iron powder, vermiculite, activated carbon, and so on) among different commercial hand warmers, comparative studies were employed to measure the impact of different commercial hand warmers. Although there are certain differences in the component contents of each commercial hand warmer, the mass percentage composition of each commercial hand warmer is generally controlled at a similar level: 70~85% iron powder, 10~20% vermiculite, 1~10% activated carbon, and a small amount of NaCl to ensure the heating. As expected, the slight difference in composition in the different commercial hand warmers caused little variation in the RhB degradation by PS (Figure S2). Therefore, the effect of the different kinds of commercial hand warmers on catalytic PS in RhB oxidation is negligible. However, all experiments were conducted using the same commercial hand warmer to maintain the consistency of the experiment in our study.

3.3. Effect of Several Parameters on the Degradation of RhB

To gain insight into the effects of reaction parameters on RhB degradation in the PS/hand warmer system, the effect of the PS concentration, the catalyst dosage, and the initial pH on the degradation of RhB were investigated. Figure 6a depicts the effect of PS concentration on the oxidation of RhB. The degradation efficiency of RhB was 98% with 1 mM PS. Hence, the degradation efficiency was slightly enhanced when the concentration of PS increased from 1 to 7 mM. Moreover, the increase in the PS concentration led to an increase in the reaction rate (Figure S3). The apparent rate constants were 11.41×10^{-2}, 36.97×10^{-2}, and 50.47×10^{-2} min^{-1} at 1, 3, and 5 mM of initial concentration of PS, due to more reactive oxidizing species ($SO_4^{\bullet-}$, $^{\bullet}OH$) produced, respectively. However, at the highest PS concentration (7 mM), a slightly decreased performance was noticed, with an apparent rate constant of 48.84×10^{-2} min^{-1}. The increment in PS has a diminishing return on the reaction rate, mainly due to the self-oxidation at higher concentrations of reactive oxidizing species inhibiting the degradation of the contaminants. This result is consistent with the previous studies that showed that an excessive amount of initial PS caused the scavenging reaction of radicals, as the following equations expressed [1,31,32]. For example, Su et al. studied the oxidative degradation of RhB with H_2O_2 activated by iron (II) tetra-(5.6-dichloro-1,4-dithiin)-porphyrazine and found that a higher concentration (7.2 mM) of H_2O_2 inhibited the oxidation of the substrate [31]. Gao et al. investigated

the kaolinite-supported iron oxide/PS/visible LED light process for the decolorization of RhB [1]. They also reported the occurrence of scavenging reactions of $SO_4^{\bullet-}$.

$$S_2O_8^{2-} + SO_4\cdot^- \rightarrow SO_4^{\bullet-} + S_2O_8^{-}\cdot + SO_4^{2-} \quad (1)$$

$$2SO_4^{\bullet-} \rightarrow S_2O_8^{2-} \quad (2)$$

$$H_2O_2 + {}^{\bullet}OH \rightarrow HOO^{\bullet} + H_2O \quad (3)$$

$${}^{\bullet}OH + HOO^{\bullet} \rightarrow O_2\cdot + H_2O \quad (4)$$

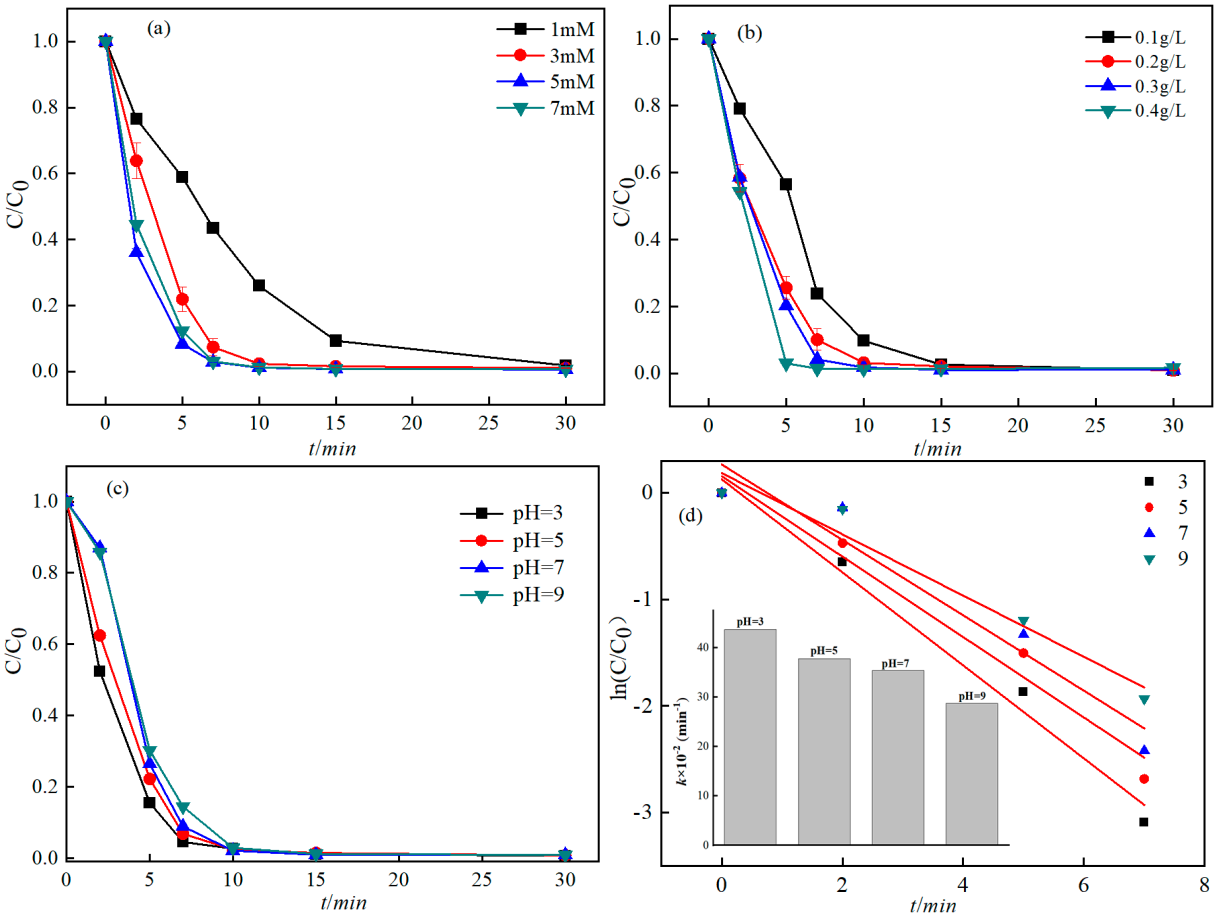

Figure 6. Effects of several parameters on the decolorization of RhB under the PS/hand warmer system: (**a**) PS concentration, (**b**) the catalyst dosage, and (**c**) the initial pH. (**d**) Comparison of the apparent rate constants for the degradation of RhB in the different initial pH conditions.

When the hand warmer dosage is raised from 0.1 to 0.4 g/L, the degradation of RhB is slightly accelerated. The apparent rate constants were 14.99×10^{-2} min^{-1}, 37.74×10^{-2} min^{-1}, 45.85×10^{-2} min^{-1}, and 57.58×10^{-2} min^{-1} for catalyst dosages ranging from 0.1 to 0.4 g/L (Figure S4), respectively. This is because a higher dosage of catalyst provides a higher specific surface area and more active sites for the generation of radicals in the degradation process. Nevertheless, there was no significant difference in the degradation efficiency of RhB in 30 min with the catalyst dosage increasing from 0.1 to 0.4 g/L (Figure 6b).

The results obtained from the RhB degradation at a series of initial pH are displayed in Figure 6c, showing the decolorization of RhB without any significant change at pH 3–9. Therefore, the hand warmer efficiently activated PS for the decolorization of RhB

over a wider pH range (3.0–9.0), when compared to the narrow pH range of 2.0–4.0 for homogeneous Fenton-like processes [33]. Consequently, the normal pH (pH = 4.5 ± 0.2) with an initial RhB concentration of 100 mg/L could be used in our experiment without any pH adjustment. In addition, Deng et al. also reported that Fe^0/PS was effective for organic degradation over a broad pH range of 3~8.5. However, the apparent rate constant of acetaminophen degradation decreased clearly from 71.04×10^{-3}, 33.08×10^{-3}, 21.49×10^{-3} to 16.13×10^{-3} min^{-1} with the increase in pH from 3, 5.5, 7 to 8.5 [13]. Contrastively, the apparent rate constants of RhB degradation with the oxidation of the hand warmer/PS system decreased slightly from 43.65×10^{-2}, 37.74×10^{-2}, 35.38×10^{-2} to 28.74×10^{-2} min^{-1} with the increase in pH from 3 to 5, 7, and 9 (Figure 6d). It is also noteworthy that there was no obvious impact on the iron leaching when the initial pH value changed in the range of 3–9 (Figure S6). The concentration of iron leached from the hand warmer was 1.07mg/L at pH = 4.5 ± 0.2. However, the concentration of iron leached from the hand warmer into the aqueous phase was 21.4 mg/L in the presence of the PS and RhB. As Figure S6 shows, the concentrations of iron leached were 23.1, 17.1, 16.5, and 19.0 mg/L with the increase in pH from 3 to 5, 7, and 9. As previously reported, the 0.8 mM of Fe^{2+} activated PS to degrade RhB (100 mg/L) with the pseudo-first-order rate constant of 14.24×10^{-2} min^{-1} at pH = 7, which would bring 44.8 mg/L iron into the solution [34]. Comparatively, the 0.2g/L of the hand warmer just leached 16.5 mg/L iron into the solution with the apparent rate constant of 35.38×10^{-2} min^{-1} at pH = 7. Hence, the hand warmer/PS process could largely enhance the degradation of RhB with low iron leaching.

3.4. Proposed Degradation Mechanisms

3.4.1. Radical Identification

Generally, the organic contaminants in the solution were destroyed by two reactive radical species ($SO_4^{\bullet-}$ and $HO^{\bullet}$) in the PS oxidation system [35–37]. Herein, to identify the dominant reactive radical species for RhB oxidation in the PS/hand warmer system, quenching experiments were performed. Due to the different reaction rates with $SO_4^{\bullet-}$ and $HO^{\bullet}$, EtOH and TBA are usually used as radical scavengers. EtOH can quench both $HO^{\bullet}$ and $SO_4^{\bullet-}$ ($k_{HO\bullet}$ = 1.6~7.7 × 10^7 $M^{-1}s^{-1}$, $k_{SO4\bullet-}$ = 1.2~2.8 × 10^9 $M^{-1}s^{-1}$) [38], while TBA is very effective for $HO^{\bullet}$ ($k_{HO\bullet}$ = 3.8~7.6 × 10^8 $M^{-1}s^{-1}$) but not very effective for $SO_4^{\bullet-}$ ($k_{SO4\bullet-}$ = 4~9.1 × 10^5 $M^{-1}s^{-1}$) [11,22]. As shown in Figure 7, the RhB exhibited various degradation performances under different concentrations of EtOH and TBA, and the inhibition was enhanced with the increase in their concentrations. The removal efficiency of RhB decreased from 99.1% to 89.9% and 37.6% in 30 min with 15 mM EtOH and 150 mM EtOH, respectively. Furthermore, the addition of 15 mM TBA led to no obvious changes in RhB degradation in 30 min, and 150 mM TBA caused a slight decrease in RhB degradation. It can be preliminarily deduced that the $SO_4^{\bullet-}$ played an important role in RhB oxidation. Then, the apparent rate constants dropped from 37.74×10^{-2} min^{-1} to 31.09×10^{-2} min^{-1} and 23.85×10^{-2} min^{-1}, respectively, due to the addition of 15 mM TBA and 150 mM TBA (Figure S5), suggesting that $HO^{\bullet}$ was also generated in the system. Therefore, both $HO^{\bullet}$ and $SO_4^{\bullet-}$ participated in the degradation of RhB, and $SO_4^{\bullet-}$ activation of PS was the dominant process.

Furthermore, the EPR measurements were used to confirm the reactive radical species involved in the PS activation process. In the EPR experiments, DMPO was employed as the spin-trapping agent to capture the radicals. As shown in Figure 8, in the presence of PS alone, slight signals for DMPO-OH and DMPO-SO_4 adducts appeared. This phenomenon could explain the slight degradation (25.7% in 30 min) of RhB induced only by the PS. With he addition of the PS/oxidized hand warmer, the EPR results were similar to those for PS alone, which revealed that the oxidized hand warmer was unable to cause PS to produce more $SO_4^{\bullet-}$. However, the intensities of the DMPO-OH and DMPO-SO_4 adducts were dramatically enhanced after the addition of PS and the hand warmer, which revealed that more radicals were formed in the PS/hand warmer system. These results further confirmed that both $HO^{\bullet}$ and $SO_4^{\bullet-}$ were generated in the PS/hand warmer system.

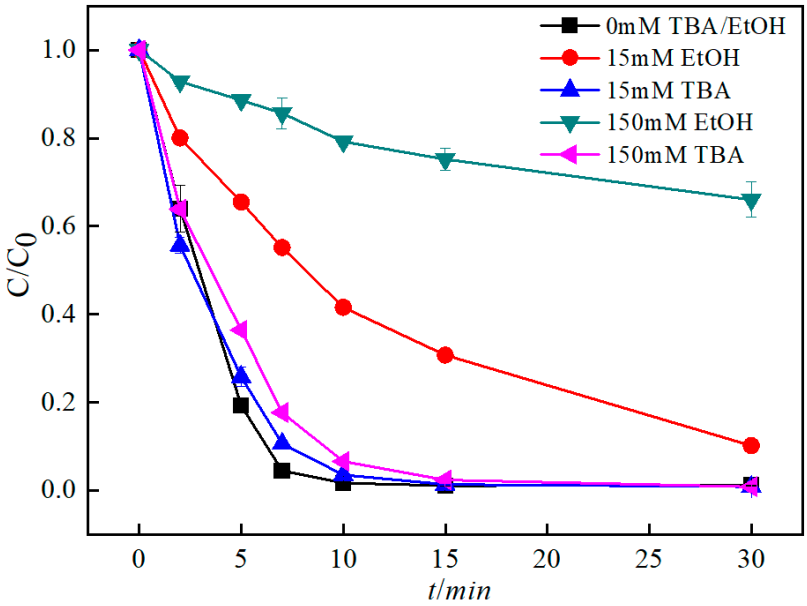

Figure 7. RhB removal in the presence of different radicals scavengers for the PS/hand warmer system. Conditions: RhB = 100 mg/L, PS = 5 mM, catalyst = 0.2 g/L, no pH adjustment.

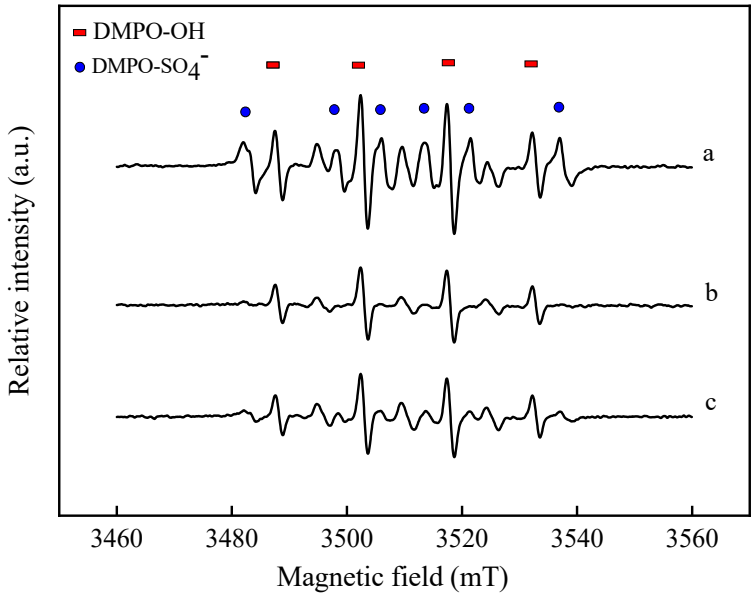

Figure 8. EPR spectra of DMPO-OH and DMPO-SO_4^- adducts for various processes: (**a**) PS/hand warmer system, (**b**) PS/oxidized hand warmer system, (**c**) PS system.

3.4.2. Proposed Degradation Pathways of RhB

The UV-vis adsorption spectra of RhB in the PS/hand warmer system are displayed in Figure 9. As reported, the degradation of RhB occurs via two competitive pathways: (i) N-de-ethylation and (ii) the destruction of the conjugated structure (he 2009, Li 2007). It was noted that two peaks of the original RhB are depicted at 259 nm (corresponding to aromatic rings) and 554 nm (corresponding to conjugated structure) [39,40]. The absorbance of the peaks at 259 nm and 554 nm decreased rapidly within 10 min, which inferred that both the aromatic rings and the conjugated structure were destroyed. No hypochromic shifts of the absorption maximum (550 nm) were observed, indicating that the formation of a series of N-de-ethylated intermediates was not reflected in the absorption spectrum [41]. Therefore, these results demonstrated that the destruction of the conjugated structure was the main pathway of RhB degradation.

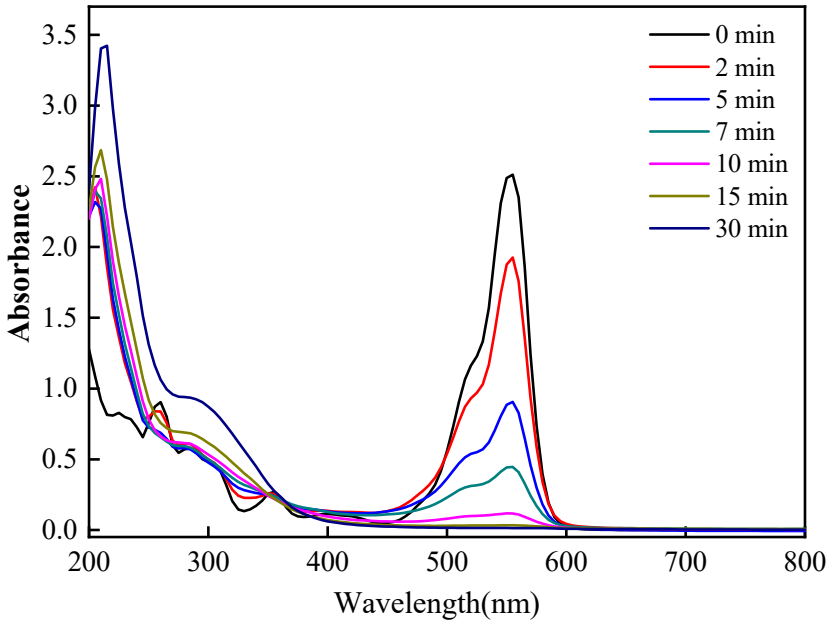

Figure 9. UV-vis spectral changes of RhB with PS/hand warmer system. Conditions: RhB = 100 mg/L, PS = 5 mM, catalyst = 0.2 g/L, no pH adjustment.

To provide further evidence that RhB had been degraded during oxidation, the mineralization degree of RhB was evaluated through determination of the variation in total organic carbon (TOC), as shown in Figure 10a. Although RhB degradation in the PS/hand warmer system occurred quickly in 10 min, the TOC removal efficiency of the RhB solution lagged behind the RhB decolorization. The degradation efficiency of RhB was 95% in 10 min, but TOC only degraded by 30%. Notably, a further decrease in TOC of approximately 14% (60 min) was observed even after complete decolorization of RhB (30 min). This might be attributed to the further oxidation of intermediates within RhB degradation. Additionally, the pH of the reaction system decreased during the RhB oxidation in the presence of PS, due to the formation of hydrogen ions (H^+) in solution (Figure 10b). As mentioned above, the activation of PS usually generates both $HO^•$ and $SO_4^{•-}$ to degrade organic compounds. The process of generating $HO^•$ is usually associated with the decrease in the solution pH because of the byproduct of H^+ (Equations (5) and (6)). In turn, the decline in pH could promote the cycling of Fe(III)/Fe(II) to generate more Fe^{2+}, further leading to the higher production of radicals.

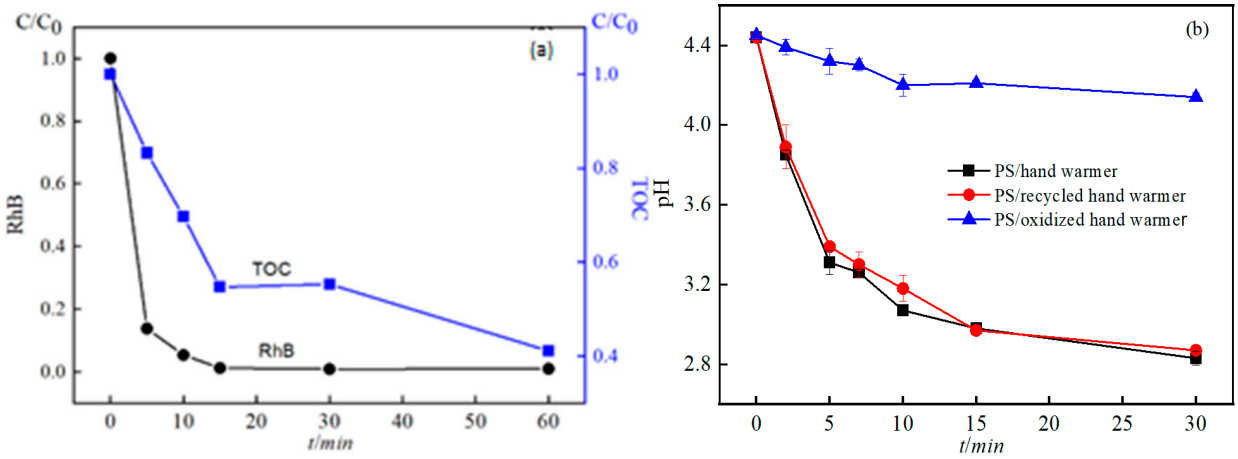

Figure 10. (**a**) Mineralization of RhB in solution at different times; (**b**) the variation in pH in the PS/hand warmer.

Acidic conditions:

$$SO_4^{\bullet-} + H_2O \rightarrow \cdot\bullet OH + H^+ + SO_4^{2-} \quad (5)$$

Alkaline conditions:

$$SO_4^{\bullet-} + OH^- \rightarrow \cdot\bullet OH + SO_4^{2-} \quad (6)$$

3.4.3. Possible Mechanism of PS Activation by Hand Warmer

In light of both $HO^{\bullet}$ and $SO_4^{\bullet-}$ participation in the PS oxidation, the possible activation mechanisms for $HO^{\bullet}$ and $SO_4^{\bullet-}$ generation were analyzed and are proposed as illustrated in Scheme 1. Based on the discussion above, the possible mechanism for PS activation by the hand warmer in the RhB degradation process is expressed as Equations (5)–(11). The Fe^0 first engendered Fe^{2+} through different reactions in different aqueous solutions to initiate a series of reactions. In an acidic solution, the iron and activated carbon formed an Fe-C micro-electrolysis system [42]. Fe^0 acts as an anode and loses electrons to form Fe^{2+}, and the H^+ gains the electrons and is transformed into H_2. The cell reactions of the Fe-C micro-electrolysis system can be represented as follows:

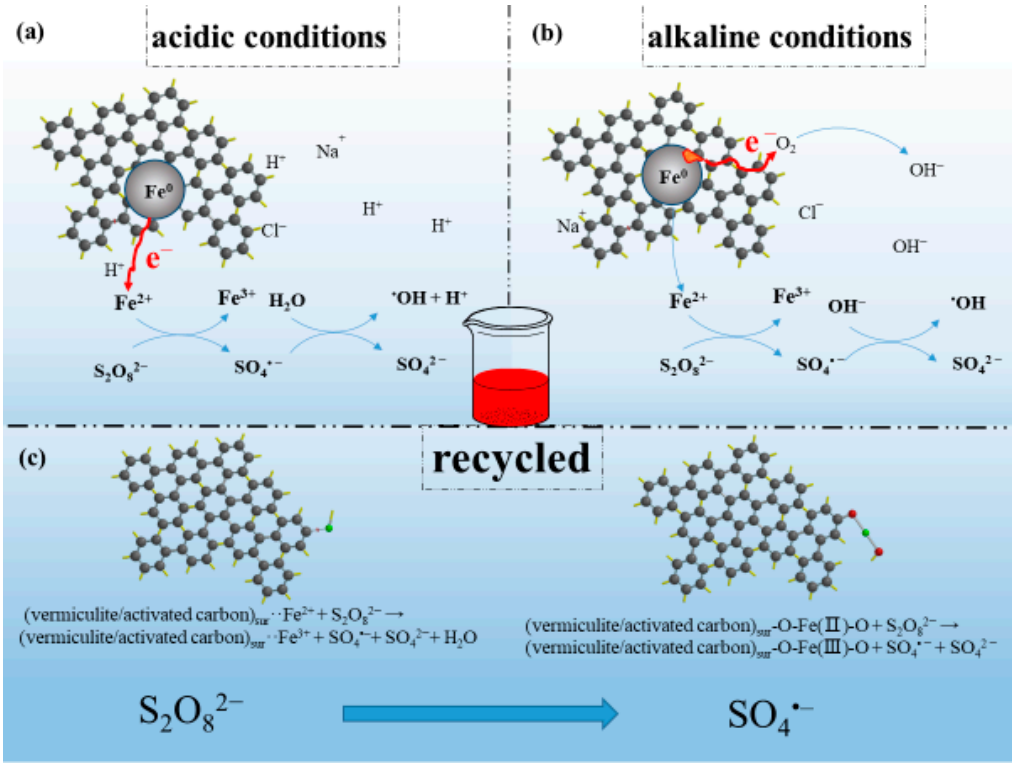

Scheme 1. Possible activation mechanisms for radical generation in RhB degradation with (**a**) hand warmer in acidic conditions, (**b**) hand warmer in alkaline conditions, and (**c**) recycled hand warmer.

Anode (acidic conditions):

$$Fe^0 - 2e^- \rightarrow Fe^{2+} \quad (7)$$

Cathode (acidic conditions):

$$2H^+ + 2e^- \rightarrow H_2 \quad (8)$$

When in alkaline conditions, the iron, activated carbon, and salt in the hand warmer together with OH^- in solution also formed many tiny micro-electrolysis systems, and the micro-electrolysis could bring about the electrical environment to promote the corrosion of

iron, which was responsible for the relatively high reaction rate of PS activation by the hand warmer in RhB degradation at pH 7–9 [43]. This is also the reason for the slight decrease in the rate constant with the increased pH in the hand warmer/PS system, compared to the obvious decreased in the Fe^0/PS system. In the electrical environment, the reaction rate slightly decreased at pH 7–9 compared to that at pH 3–5, because the increase in pH led to the decrease in electric potential difference and inhibited the production of radicals. Specifically, the Fe^0 loses electrons and transforms into Fe^{2+} in the electrical environment (Equation (9)). The O_2 gains the electrons and transforms into OH^- (Equation (10)).

Anode (alkaline conditions):

$$2Fe^0 - 4e^- \rightarrow 2Fe^{2+} \quad (9)$$

Cathode (alkaline conditions):

$$O_2 + 4e^- + 2H_2O \rightarrow 4OH^- \quad (10)$$

Then, the Fe^{2+} also catalyzed PS to generate $SO_4^{\bullet-}$.

$$Fe^{2+} + 2S_2O_8^{2-} \rightarrow Fe^{3+} + SO_4^{\bullet-} + SO_4^{2-} \quad (11)$$

Simultaneously, the produced $SO_4^{\bullet-}$ can be converted into $^{\bullet}OH$ in the PS/hand warmer system through Equations (5) or (6). The reactive radical species of $SO_4^{\bullet-}$ and $^{\bullet}OH$ attack the conjugated structure of RhB and decompose RhB into several intermediates, which are finally mineralized into CO_2 and H_2O through a series of reactions (Equation (12)).

$$^{\bullet}OH\cdot/SO_4^{\bullet-} + RhB \rightarrow \text{intermediates} \rightarrow CO_2 + H_2O \quad (12)$$

3.5. Reusability of Hand Warmer

From a sustainable economic perspective, the reusability of the catalyst is crucial for its practical application. The operational reusability and stability of the hand warmer were explored through three consecutive experiments. The recycled catalyst was removed from the reaction mixture at the end of each oxidation process, then washed with distilled water and dried in an air-dry oven for the next oxidation experiment. As shown in Figure 11, the activity of the recycled catalyst had no significant change after each run, indicating the high stability and reusability of the hand warmer.

To explore the mechanism of the material reusability, the UV-vis adsorption spectra of RhB in the PS/1st recycled hand warmer system were also tested, which are shown in Figure S7. Similarly, the conjugated structure of the RhB was destroyed within the 1st recycled hand warmer/activated PS run. The quenching experiments of the PS/1st recycled hand warmer system (Figure S8) showed that the 1st recycled hand warmer also catalyzed PS to produce HO• and $SO_4^{\bullet-}$ in the degradation of RhB. Therefore, the mechanism for PS-oxidized RhB through 1st recycled hand warmer activation is the same as hand warmer activation.

In general, zero-valent iron can be dissolved in an aqueous solution under acidic conditions. As a result, the iron-content catalyst loses reusability after reaction under acidic conditions, and the recycled materials cannot activate PS [13]. Interestingly, the hand warmer retained reusability with the initial pH (pH = 4.5 ± 0.2) in our study. To explain this reusable phenomenon, the XPS and FTIR techniques helped to provide evidence for the reusability of the recycled hand warmer. As Figure S9 exhibits, compared to the hand warmer, the Fe 2p spectra of the recycled hand warmer consisted of Fe^{3+} $2p_{3/2}$, Fe^{3+} $2p_{1/2}$, and satellite Fe^{3+} peaks. Moreover, a satellite Fe^{2+} peak located at 714.6 eV emerged, which confirmed the existence of Fe^{2+} species on the surface of the recycled material [20]. Thus, the presence of the Fe^{2+} gives the recycled hand warmer capability to activate PS. The C1s spectra also showed that there are -COOH, C-O, and C-C (-CH, CH_2, CH_3) groups

on the surface of the 1st recycled hand warmer. In the FTIR spectra of the 1st recycled hand warmer (Figure S10), there are two obvious absorption peaks at 3399.21 cm^{-1} and 1004.43 cm^{-1}, corresponding to the -OH and C-O groups, respectively, and the intensity of these two absorption peaks increased significantly compared with the hand warmer.

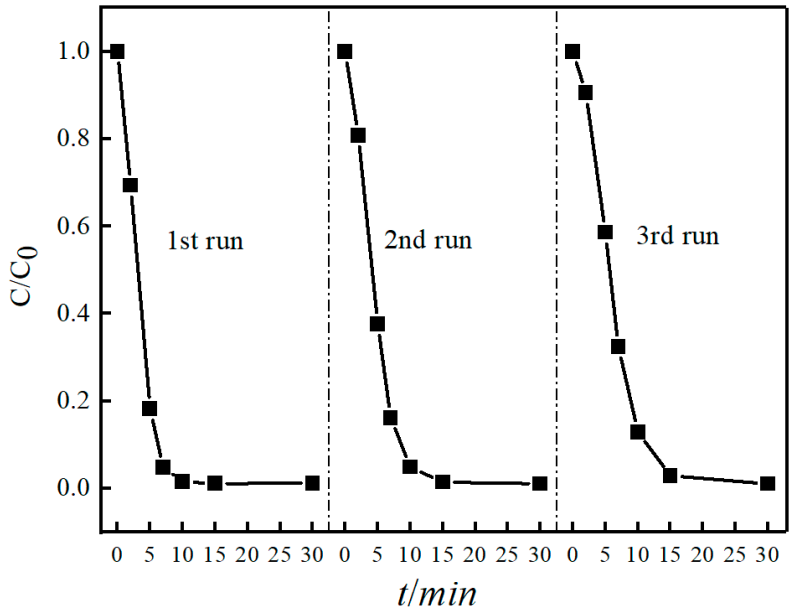

Figure 11. The reusability of the hand warmer. Reaction conditions: RhB 100 mg/L; PS 5 mM; hand warmer 0.4 g/L; no pH adjustment.

In conclusion, the reusability of the hand warmer might be attributed to two possible reasons: (1) the Fe^{2+} adsorbed on vermiculite/activated carbon forms (vermiculite/activated carbon)$_{sur}$··Fe^{2+}, which activates PS to generate $SO_4^{\bullet-}$ in RhB degradation (Equation (13)). Consequently, the iron ion adsorbed on the vermiculite/activated carbon makes the hand warmer material stable and reusable. (2) The emergence of Fe^{2+} and the increase in -OH and -C-O groups might correspond to the C-O-Fe(II) group on the surface of the recycled hand warmer, which could catalyze PS to degrade RhB. As previously reported, the iron species could react with the surface functional groups (-OH, -COOH, and so on) of the vermiculite/activated carbon and form the (vermiculite/activated carbon)$_{sur}$-OFeO species [21]. Furthermore, the (vermiculite/activated carbon)$_{sur}$-OFeO species could serve as the activation segment to catalyze PS for producing radicals. Consequently, the (vermiculite/activated carbon)$_{sur}$-OFeO species react with PS as expressed in Equation (14).

$$\text{(vermiculite/activated carbon)}_{sur}\cdot\cdot Fe^{2+} + S_2O_8^{2-} \rightarrow \text{(vermiculite/activated carbon)}_{sur}\cdot\cdot Fe^{3+} + SO_4^{\bullet-} + SO_4^{2-} + H_2O \quad (13)$$

$$\text{(vermiculite/activated carbon)}_{sur}\text{-O-Fe(II)-O} + S_2O_8^{2-} \rightarrow \text{(vermiculite/activated carbon)}_{sur}\text{-O-Fe(III)-O} + SO_4^{\bullet-} + SO_4^{2-} \quad (14)$$

Overall, these two possible reasons reveal that the other components (vermiculite/activated carbon) within the hand warmer may be responsible for the reusability and stability.

3.6. Comparison of the Degradation of RhB through Different Processes

As shown in Table 1, we compared the degradation of RhB in the PS process with different catalysts. The dosage of PS was only 3 mM in our hand warmer/PS process, while the PS dosage of other catalysts was above 8mM, and the reaction rate constants of RhB removal in these processes (0.010–0.233 min^{-1}) were much lower than those in the hand warmer/PS process (0.354 min^{-1}) at a high concentration of RhB and pH 7. If the dosage of PS increased, the reaction rate would be faster. The reason for the faster reaction rate of the hand warmer may be the formation of many tiny micro-electrolysis systems,

and the micro-electrolysis could bring about the electrical environment to promote the reaction rate of PS activation in RhB degradation at pH 7. In addition, our hand warmer/PS process presented a high pH working range, even working at pH 9 (28.74 min^{-1}). Generally, catalysts such as Fe^0, Fe^{2+}, and pre-Fe^0 will dissolve into the solution during oxidation and cannot be reused. Nevertheless, the hand warmer is easily removed from the reactor at the end of each oxidation process and then can be repetitively used. Therefore, the hand warmer/PS process showed an advantage over other PS-based processes for the degradation of RhB.

Table 1. Comparison of the degradation of RhB through different processes.

Type of Process	Catalyst (g L^{-1})	PS (mM)	RhB (mg L^{-1})	pH	Reaction Rate Constant (min^{-1})	Reusability of Catalyst	Ref.
Pyrite/PS	1	8	20	3	0.031	No	[44]
Fe_3O_4/PS	10	12	76	3.5	0.01	Yes	[28]
Fe^0/PS	0.224	8	100	7	0.094	No	[34]
Fe^{2+}/PS	0.224	8	100	7	0.142	No	[34]
Pre-Fe^0/PS	0.224	8	100	7	0.233	No	[34]
Hand warmer/PS	0.2	3	100	7	0.354	Yes	This study

4. Conclusions

A novel method for RhB degradation in a heterogeneous activation system of PS and a hand warmer was investigated. The results showed that the degradation efficiencies of RhB were maintained above 90% in 30 min by using 0.1~0.4 g/L of hand warmer to activate 3 mM PS. The heterogeneous process was suitable for a wide range of pH (pH 3.0–9.0) conditions in solution. The iron in the hand warmer is the main active ingredient that catalyzes PS, and the formation of micro-batteries with iron, activated carbon, salt, and H^+/OH^- accelerates the activation reaction in solution. Based on the quenching experiments and EPR results, the $HO^•$ and $SO_4^{•-}$ were the two main reactive oxygen species in the hand warmer/PS process. The generated $HO^•$ and $SO_4^{•-}$ destroyed the conjugated structure of RhB and decomposed RhB into several intermediates. Moreover, the hand warmer could be reused several times to activate PS. Therefore, this study gives an in-depth insight into further reusable mechanism studies of hand warmers. This work exhibits a promising hand warmer catalyst for efficient RhB removal and provides new insights into the activation mechanism of PS by hand warmers.

Supplementary Materials: The following supplementary materials can be downloaded at: https://www.mdpi.com/article/10.3390/su151713034/s1, Figure S1: The apparent rate constants for the process of PS/ hand warmer and PS; Figure S2: Comparative study of RhB degradation using three different commercial hand warmers; Figure S3: Comparison of the apparent rate constants for the decolorization of RhB in the different PS concentrations; Figure S4: Comparison of the apparent rate constants for the decolorization of RhB in the different catalyst dosages; Figure S5: The apparent rate constants for the degradation of RhB in the presence of different radical scavengers in the PS/ hand warmer system; Figure S6: The concentration of leached iron at different solution pH; Figure S7: UV-vis spectral changes of RhB with PS/ 1st recycled hand warmer system; Figure S8: RhB removal in the presence of different radicals scavengers; Figure S9: XPS profiles of the surface of recycled hand warmer; Figure S10: FTIR spectra of hand warmer and recycled hand warmer.

Author Contributions: T.Y.: Conceptualization, Investigation, Writing—original draft, Data curation, Validation. L.L. and Y.W.: Investigation, Data curation, Validation. C.L. and H.L.: Validation. Z.W.: Supervision, Resources, Visualization. J.Z.: Supervision, Writing—review and editing, Visualization, Resources. All authors have read and agreed to the published version of the manuscript.

Funding: This work was jointly supported by the National Environmental Protection Public Welfare Industry Targeted Research Fund (PM-zx703-202204-069), Guangzhou Science and Technology Plan (202102080209).

Institutional Review Board Statement: Not applicable.

Informed Consent Statement: Not applicable.

Data Availability Statement: Data will be made available on request.

Conflicts of Interest: No potential conflict of interest are reported by the authors.

References

1. Gao, Y.; Zhang, Z.; Li, S.; Liu, J.; Yao, L.; Li, Y.; Zhang, H. Insights into the mechanism of heterogeneous activation of persulfate with a clay/iron-based catalyst under visible LED light irradiation. *Appl. Catal. B Environ.* **2016**, *185*, 22–30. [CrossRef]
2. Antonopoulou, M.; Evgenidou, E.; Lambropoulou, D.; Konstantinou, I. A review on advanced oxidation processes for the removal of taste and odor compounds from aqueous media. *Water Res.* **2014**, *53*, 215–234. [CrossRef] [PubMed]
3. Neta, P.; Huie, R.E.; Ross, A.B. Rate constants for reactions of inorganic radicals in aqueous solution. *J. Phys. Chem. Ref. Data* **1988**, *17*, 1027–1284. [CrossRef]
4. Mohod, A.V.; Momotko, M.; Shah, N.S.; Marchel, M.; Imran, M.; Kong, L.; Boczkaj, G. Degradation of Rhodamine dyes by Advanced Oxidation Processes (AOPs)–Focus on cavitation and photocatalysis—A critical review. *Water Resour. Ind.* **2023**, *30*, 1–30. [CrossRef]
5. Ahmed, M.M.; Chiron, S. Solar photo-Fenton like using persulphate for carbamazepine removal from domestic wastewater. *Water Res.* **2014**, *48*, 229–236. [CrossRef]
6. Anipsitakis, G.P.; Dionysiou, D.D.; Gonzalez, M.A. Cobalt-mediated activation of peroxymonosulfate and sulfate radical attack on phenolic compounds. implications of chloride ions. *Environ. Sci. Technol.* **2006**, *40*, 1000–1007. [CrossRef]
7. Guo, Y.; Zeng, Z.; Zhu, Y.; Huang, Z.; Cui, Y.; Yang, J. Catalytic oxidation of aqueous organic contaminants by persulfate activated with sulfur-doped hierarchically porous carbon derived from thiophene. *Appl. Catal. B Environ.* **2018**, *220*, 635–644. [CrossRef]
8. Rodriguez, S.; Vasquez, L.; Costa, D.; Romero, A.; Santos, A. Oxidation of Orange G by persulfate activated by Fe(II), Fe(III) and zero valent iron (ZVI). *Chemosphere* **2014**, *101*, 86–92. [CrossRef]
9. Gao, Y.; Luo, J.; Song, T.; Yu, X. Research progress on nano-Fe^0/PS system for degradation of refractory organics in aqueous solution. *J. Environ. Chem. Eng.* **2021**, *9*, 105345. [CrossRef]
10. Zhang, Y.; Ma, Z.; Xie, X.; Wu, D.; Peng, X.; Li, J. Mechanochemically synthesized silicotungsten acidified ZVI composite for persulfate activation: Enhancement of the electron transfer and Fe slowly release mechanism. *Chemosphere* **2023**, *336*, 139254. [CrossRef]
11. Ji, Y.; Ferronato, C.; Salvador, A.; Yang, X.; Chovelon, J.M. Degradation of ciprofloxacin and sulfamethoxazole by ferrous-activated persulfate: Implications for remediation of groundwater contaminated by antibiotics. *Sci. Total Environ.* **2014**, *472*, 800–808. [CrossRef] [PubMed]
12. Cao, J.; Zhang, W.-X.; Brown, D.G.; Sethi, D. Oxidation of lindane with Fe(II)-activated sodium persulfate. *Environ. Eng. Sci.* **2008**, *25*, 221–228. [CrossRef]
13. Deng, J.; Shao, Y.; Gao, N.; Deng, Y.; Tan, C.; Zhou, S. Zero-valent iron/persulfate(Fe^0/PS) oxidation acetaminophen in water. *Int. J. Environ. Sci. Technol.* **2013**, *11*, 881–890. [CrossRef]
14. Zhang, X.; Feng, M.; Qu, R.; Liu, H.; Wang, L.; Wang, Z. Catalytic degradation of diethyl phthalate in aqueous solution by persulfate activated with nano-scaled magnetic $CuFe_2O_4$ /MWCNTs. *Chem. Eng. J.* **2016**, *301*, 1–11. [CrossRef]
15. Herney-Ramirez, J.; Vicente, M.A.; Madeira, L.M. Heterogeneous photo-Fenton oxidation with pillared clay-based catalysts for wastewater treatment: A review. *Appl. Catal. B Environ.* **2010**, *98*, 10–26. [CrossRef]
16. Wang, X.; Zhou, Y.; Ndayiragije, S.; Wang, N.; Tang, H.; Zhu, L. Advanced oxidative degradation of sulfamethoxazole by using bowl-like $FeCuS@Cu_2S@Fe^0$ catalyst to efficiently activate peroxymonosulfate. *J. Environ. Sci.* **2023**, *126*, 348–364. [CrossRef]
17. Tam, A.Y.B.; Chan, Y.C.; Lau, F.L. A case series of accidental ingestion of hand warmer. *Clin. Toxicol.* **2008**, *46*, 900–904. [CrossRef]
18. Lee, Y.-J.; Lee, C.-G.; Park, S.-J.; Jho, E.H. Degradation of Oxytetracycline by Persulfate Activation Using a Magnetic Separable Iron Oxide Catalyst Derived from Hand-Warmer Waste. *Appl. Sci.* **2021**, *11*, 10447. [CrossRef]
19. Yang, S.; Yang, X.; Shao, X.; Niu, R.; Wang, L. Activated carbon catalyzed persulfate oxidation of Azo dye acid orange 7 at ambient temperature. *J. Hazard. Mater.* **2011**, *186*, 659–666. [CrossRef]
20. Bhargava, G.; Gouzman, I.; Chun, C.M.; Ramanarayanan, T.A.; Bernasek, S.L. Characterization of the "native" surface thin film on pure polycrystalline iron: A high resolution XPS and TEM study. *Appl. Surf. Sci.* **2007**, *253*, 4322–4329. [CrossRef]
21. Luo, H.; Lin, Q.; Zhang, X.; Huang, Z.; Liu, S.; Jiang, J.; Xiao, R.; Liao, X. New insights into the formation and transformation of active species in nZVI/BC activated persulfate in alkaline solutions. *Chem. Eng. J.* **2019**, *359*, 1215–1223. [CrossRef]
22. Tang, L.; Liu, Y.; Wang, J.; Zeng, G.; Deng, Y.; Dong, H.; Feng, H.; Wang, J.; Peng, B. Enhanced activation process of persulfate by mesoporous carbon for degradation of aqueous organic pollutants: Electron transfer mechanism. *Appl. Catal. B Environ.* **2018**, *231*, 1–10. [CrossRef]
23. Wang, X.; Du, Y.; Liu, H.; Ma, J. Ascorbic acid/Fe^0 composites as an effective persulfate activator for improving the degradation of rhodamine B. *RSC Adv.* **2018**, *8*, 12791–12798. [CrossRef] [PubMed]
24. Solum, M.S.; Pugmire, R.J.; Jagtoyen, M. Evolution of carbon structure in chemically activated wood. *Carbon* **1995**, *33*, 1247–1254. [CrossRef]
25. Chen, J.; Hong, W.; Huang, T.; Zhang, L.; Li, W.; Wang, Y. Activated carbon fiber for heterogeneous activation of persulfate: Implication for the decolorization of azo dye. *Environ. Sci. Pollut. Res. Int.* **2016**, *23*, 18564–18574. [CrossRef] [PubMed]

26. Laokul, P.; Amornkitbamrung, V.; Seraphin, S.; Maensiri, S. Characterization and magnetic properties of nanocrystalline $CuFe_2O_4$, $NiFe_2O_4$, $ZnFe_2O_4$ powders prepared by the Aloe vera extract solution. *Curr. Appl. Phys.* **2011**, *11*, 101–108. [CrossRef]
27. Selvan, R.K.; Augustin, C.; Berchmans, L.J.; Saraswathi, R. Combustion synthesis of $CuFe_2O_4$. *Mater. Res. Bull.* **2003**, *38*, 41–54. [CrossRef]
28. Leng, Y.; Guo, W.; Shi, X.; Li, Y.; Xing, L. Polyhydroquinone-coated Fe_3O_4 nanocatalyst for degradation of rhodamine B based on sulfate radicals. *Ind. Eng. Chem. Res.* **2013**, *52*, 13607–13612. [CrossRef]
29. Liu, Y.; Guo, H.; Zhang, Y.; Cheng, X.; Zhou, P.; Zhang, G.; Wang, J.; Tang, P.; Ke, T.; Li, W.J.S.; et al. Heterogeneous activation of persulfate for rhodamine B degradation with 3D flower sphere-like BiOI/Fe_3O_4 microspheres under visible light irradiation. *Sep. Purif. Technol.* **2018**, *192*, 88–98. [CrossRef]
30. Ahangaran, F.; Hassanzadeh, A.; Nouri, S. Surface modification of Fe_3O_4@SiO_2 microsphere by silane coupling agent. *Int. Nano Lett.* **2013**, *3*, 1–5. [CrossRef]
31. Su, R.; Sun, J.; Sun, Y.; Deng, K.; Cha, D.; Wang, D. Oxidative degradation of dye pollutants over a broad pH range using hydrogen peroxide catalyzed by $FePz(dtnCl_2)_4$. *Chemosphere* **2009**, *77*, 1146–1151. [CrossRef] [PubMed]
32. Avetta, P.; Pensato, A.; Minella, M.; Malandrino, M.; Maurino, V.; Minero, C.; Hanna, K.; Vione, D. Activation of persulfate by irradiated magnetite: Implications for the degradation of phenol under heterogeneous photo-fenton-like conditions. *Environ. Sci. Technol.* **2015**, *49*, 1043–1050. [CrossRef]
33. Kallel, M.; Belaid, C.; Boussahel, R.; Ksibi, M.; Montiel, A.; Elleuch, B. Olive mill wastewater degradation by Fenton oxidation with zero-valent iron and hydrogen peroxide. *J. Hazard. Mater.* **2009**, *163*, 550–554. [CrossRef] [PubMed]
34. Pan, Y.; Zhou, M.; Zhang, Y.; Cai, J.; Li, B.; Sheng, X.J.S.; Technology, P. Enhanced degradation of Rhodamine B by pre-magnetized Fe^0/PS process: Parameters optimization, mechanism and interferences of ions. *Sep. Purif. Technol.* **2018**, *203*, 66–74. [CrossRef]
35. Feng, M.; Qu, R.; Zhang, X.; Sun, P.; Sui, Y.; Wang, L.; Wang, Z.J.W.R. Degradation of flumequine in aqueous solution by persulfate activated with common methods and polyhydroquinone-coated magnetite/multi-walled carbon nanotubes catalysts. *Water Res.* **2015**, *85*, 1–10. [CrossRef]
36. Qi, C.; Liu, X.; Lin, C.; Zhang, X.; Ma, J.; Tan, H.; Ye, W. Degradation of sulfamethoxazole by microwave-activated persulfate: Kinetics, mechanism and acute toxicity. *Chem. Eng. J.* **2014**, *249*, 6–14. [CrossRef]
37. Liang, C.; Su, H.-W. Identification of sulfate and hydroxyl radicals in thermally activated persulfate. *Ind. Eng. Chem. Res.* **2009**, *48*, 5558–5562. [CrossRef]
38. Anipsitakis, G.P.; Dionysiou, D.D. Radical generation by the interaction of transition metals with common oxidants. *Environ. Sci. Technol.* **2004**, *38*, 3705–3712. [CrossRef]
39. Jiang, L.; Zhang, Y.; Zhou, M.; Liang, L.; Li, K. Oxidation of Rhodamine B by persulfate activated with porous carbon aerogel through a non-radical mechanism. *J. Hazard. Mater.* **2018**, *358*, 53–61. [CrossRef]
40. He, Z.; Yang, S.; Ju, Y.; Sun, C. Microwave photocatalytic degradation of Rhodamine B using TiO_2 supported on activated carbon: Mechanism implication. *J. Environ. Sci.* **2009**, *21*, 268–272. [CrossRef]
41. Chen, C.; Zhao, W.; Lei, P.; Zhao, J.; Serpone, N. Photosensitized degradation of dyes in polyoxometalate solutions versus TiO_2 dispersions under visible-light irradiation: Mechanistic implications. *Chemistry* **2004**, *10*, 1956–1965. [CrossRef] [PubMed]
42. Li, P.; Liu, Z.; Wang, X.; Guo, Y.; Wang, L. Enhanced decolorization of methyl orange in aqueous solution using iron–carbon micro-electrolysis activation of sodium persulfate. *Chemosphere* **2017**, *180*, 100–107. [CrossRef] [PubMed]
43. Zhang, W.; Li, X.; Yang, Q.; Wang, D.; Wu, Y.; Zhu, X.; Wei, J.; Liu, Y.; Hou, L.; Chen, C. Pretreatment of landfill leachate in near-neutral pH condition by persulfate activated Fe-C micro-electrolysis system. *Chemosphere* **2019**, *216*, 749–756. [CrossRef]
44. Diao, Z.-H.; Liu, J.-J.; Hu, Y.-X.; Kong, L.-J.; Jiang, D.; Xu, X.-R. Comparative study of Rhodamine B degradation by the systems pyrite/H_2O_2 and pyrite/persulfate: Reactivity, stability, products and mechanism. *Sep. Purif. Technol.* **2017**, *184*, 374–383. [CrossRef]